Molecular Biophysics:

Structural Features of Membrane-bound Glucocerebrosidase and α-Synuclein Probed by Neutron Reflectometry and Fluorescence Spectroscopy

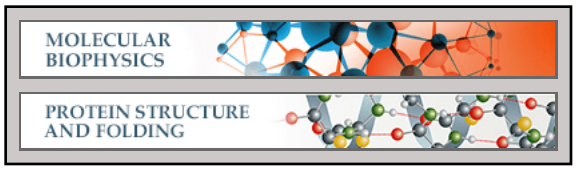

Thai Leong Yap, Zhiping Jiang, Frank Heinrich, James M. Gruschus, Candace M. Pfefferkorn, Marilia Barros, Joseph E. Curtis, Ellen Sidransky and Jennifer C. Lee

J. Biol. Chem. 2015, 290:744-754.
doi: 10.1074/jbc.M114.610584 originally published online November 26, 2014

THE JOURNAL OF BIOLOGICAL CHEMISTRY VOL. 290, NO. 2, pp. 744–754, January 9, 2015
Published in the U.S.A.

Structural Features of Membrane-bound Glucocerebrosidase and α-Synuclein Probed by Neutron Reflectometry and Fluorescence Spectroscopy*

Received for publication, September 11, 2014, and in revised form, November 17, 2014 Published, JBC Papers in Press, November 26, 2014, DOI 10.1074/jbc.M114.610584

Thai Leong Yap[‡1], Zhiping Jiang[‡1], Frank Heinrich[§¶], James M. Gruschus[‡], Candace M. Pfefferkorn[‡], Marilia Barros[§], Joseph E. Curtis[¶], Ellen Sidransky[‖], and Jennifer C. Lee[‡2]

From the [‡]Laboratory of Molecular Biophysics, NHLBI, and the [‖]Medical Genetics Branch, NHGRI, National Institutes of Health, Bethesda, Maryland 20892, the [§]Department of Physics, Carnegie Mellon University, Pittsburgh, Pennsylvania 15213, and the [¶]Center for Neutron Research, National Institute of Standards and Technology (NIST), Gaithersburg, Maryland 20899

Background: A specific interaction exists between α-synuclein and glucocerebrosidase on the lipid membrane, resulting in enzyme inhibition.
Results: Binding glucocerebrosidase has a profound effect on α-synuclein, moving roughly half of its embedded helical region above the membrane plane.
Conclusion: A model is proposed with structural insights into glucocerebrosidase inhibition by α-synuclein.
Significance: α-Synuclein-glucocerebrosidase interaction provides a molecular connection between Parkinson and Gaucher diseases.

Mutations in glucocerebrosidase (GCase), the enzyme deficient in Gaucher disease, are a common genetic risk factor for the development of Parkinson disease and related disorders, implicating the role of this lysosomal hydrolase in the disease etiology. A specific physical interaction exists between the Parkinson disease-related protein α-synuclein (α-syn) and GCase both in solution and on the lipid membrane, resulting in efficient enzyme inhibition. Here, neutron reflectometry was employed as a first direct structural characterization of GCase and α-syn·GCase complex on a sparsely-tethered lipid bilayer, revealing the orientation of the membrane-bound GCase. GCase binds to and partially inserts into the bilayer with its active site most likely lying just above the membrane-water interface. The interaction was further characterized by intrinsic Trp fluorescence, circular dichroism, and surface plasmon resonance spectroscopy. Both Trp fluorescence and neutron reflectometry results suggest a rearrangement of loops surrounding the catalytic site, where they extend into the hydrocarbon chain region of the outer leaflet. Taking advantage of contrasting neutron scattering length densities, the use of deuterated α-syn *versus* protiated GCase showed a large change in the membrane-bound structure of α-syn in the complex. We propose a model of α-syn·GCase on the membrane, providing structural insights into inhibition of GCase by α-syn. The interaction displaces GCase away from the membrane, possibly impeding substrate access and perturbing the active site. GCase greatly alters membrane-bound α-syn, moving helical residues away from the bilayer, which could impact the degradation of α-syn in the lysosome where these two proteins interact.

Mutations in *SNCA*, the gene encoding for α-synuclein (α-syn),[3] are linked to familial, early onset Parkinson disease (PD) (1–3), implicating this neuronal membrane-binding protein (4) as a pathogenic agent (5). Intracellular inclusions of fibrillar α-syn known as Lewy bodies are classic hallmarks of PD, and recently, glucocerebrosidase (GCase), a lysosomal hydrolase, has also been observed in them (6). Emerging data from numerous studies indicate a correlation between GCase deficiency and increased levels of α-syn (7–9). Importantly, mutations in *GBA1*, the gene encoding for GCase, are currently recognized as the most common risk factor for PD development (10) and recently have also been substantiated for dementia with Lewy bodies (11). Mutations in *GBA1* also cause the lysosomal storage disorder Gaucher disease; it remains an open question as to how these two diseases may be linked (12).

GCase is a 497-residue lysosomal glycoprotein that catalyzes the hydrolysis of glucosylceramide into glucose and ceramide. Both anionic phospholipids and the activator protein, saposin C (Sap C), are considered vital for maximal catalytic activity (13–17); however, the presence of either alone is sufficient to promote enzyme function *in vitro*.

In our work (18, 19), we have demonstrated an intimate molecular relationship by identifying a specific interaction between

* This work was supported by the Intramural Research Program at the National Institutes of Health, NHLBI, and NHGRI. Research was performed in part at the NIST Center for Nanoscale Science and Technology and by the NIST IMS program "Precision Measurements for Integral Membrane Proteins."
[1] Both authors contributed equally to this work.
[2] To whom correspondence may be addressed: Laboratory of Molecular Biophysics, NHLBI, National Institutes of Health, 50 South Dr., Bldg. 50 Rm. 3513, Bethesda, MD 20892. Tel.: 301-496-3741; E-mail: leej4@mail.nih.gov.

[3] The abbreviations used are: α-syn, α-synuclein; PD, Parkinson disease; GCase, glucocerebrosidase; Sap C, saposin C; NR, neutron reflectometry; stBLM, sparsely tethered bilayer lipid membrane; d-α-syn, deuterated α-synuclein; POPC, 1-palmitoyl-2-oleoyl-*sn*-glycero-3-phosphocholine; POPS, 1-palmitoyl-2-oleoyl-*sn*-glycero-3-phospho-L-serine; Br_{6-7}, 1-palmitoyl-2-(6,7-dibromo) stearoyl-*sn*-glycero-3-phosphocholine; Br_{9-10}, 1-palmitoyl-2-(9,10-dibromo)stearoyl-*sn*-glycero-3-phosphocholine; Br_{11-12}, 1-palmitoyl-2-(11,12-dibromo)stearoyl-*sn*-glycero-3-phosphocholine; SAM, self-assembled monolayer; SPR, surface plasmon resonance; nSLD, neutron scattering length density.

α-syn and GCase under the acidic solution conditions found in lysosomes, a site of α-syn degradation (20, 21) and where GCase functions. Using site-specific fluorescence and Förster energy transfer probes (19), we found that α-syn-GCase interaction on the membrane surface involves both the N- and C-terminal portions of α-syn in contrast to that found in solution, which is specific only for the last 23 residues. Intriguingly, α-syn acts as a potent mixed inhibitor of GCase *in vitro* (19), but in the presence of its cofactor Sap C, GCase activity is fully rescued (22). Although the specific role of GCase activity in modulating α-syn levels remains controversial, this apparent reciprocal relationship is paving the way toward new PD treatments. For example, viral vector-mediated increase in wild-type GCase levels was shown to reverse PD-related features in a Gaucher disease mouse model (23, 24), evidence that enhancing GCase activity is a potential therapeutic strategy for synucleinopathies.

Here, we sought to gain structural information on the membrane-bound α-syn·GCase complex. Although there are extensive structural studies on the nature of α-syn membrane interaction (4), little is known on how GCase associates with the membrane, although x-ray crystal structures of soluble GCase are available (25). We have employed neutron reflectometry (NR) to investigate the structural features of the two proteins on a sparsely tethered bilayer lipid membrane (stBLM) (26, 27). NR is unique among available techniques in that it allows the structural characterization of membrane-associated proteins bound to actual lipid bilayers in an aqueous environment (28, 29), as opposed to proteins in solid state or detergent-solubilized forms currently prevalent in the field.

The reflection of neutrons from stBLMs simultaneously probes the protein and the bilayer and readily distinguishes the layers of lipid acyl chains and phospholipid headgroups as well as the membrane-bound proteins (30–36). Both the extent of polypeptide insertion into the bilayer and extension into the aqueous surrounding can be measured. Although it is of lower resolution than some structural methods, such as x-ray crystallography and solid-state nuclear magnetic resonance spectroscopy, NR has been successfully used to characterize a number of peripheral (*e.g.* α-syn (34), HIV-1 matrix (33), colicin N (35), PTEN tumor suppressor (30), and the GRASP Golgi stacking protein (31)) and integral membrane proteins (*e.g.* hemolysin (32) and outer membrane protein F (35)) on physiologically relevant, fluid phospholipid bilayers. By exploiting the high sensitivity of neutron scattering length density differences for deuterated α-syn (d-α-syn) *versus* protiated GCase, the location of α-syn within the complex in the phospholipid bilayer was determined. Based on the orientation of GCase obtained from NR and other complementary techniques, including intrinsic Trp fluorescence and circular dichroism (CD) spectroscopy, an interaction model is proposed.

EXPERIMENTAL PROCEDURES

Materials—All lipids (1-palmitoyl-2-oleoyl-*sn*-glycero-3-phosphocholine (POPC), 1-palmitoyl-2-oleoyl-*sn*-glycero-3-phospho-L-serine (sodium salt) (POPS), 1-palmitoyl-2-(6,7 dibromo)stearoyl-*sn*-glycero-3-phosphocholine (Br_{6-7}), 1-palmitoyl-2-(9,10-dibromo)stearoyl-*sn*-glycero-3-phosphocholine (Br_{9-10}), and 1-palmitoyl-2-(11,12-dibromo)stearoyl-*sn*-glycero-3-phosphocholine (Br_{11-12})) were purchased from Avanti Polar Lipids, Inc. (Alabaster, AL) and used as received. All other chemicals were purchased from Sigma-Aldrich unless otherwise stated. Certain commercial materials, equipment, and instruments are identified in this work to describe the experimental procedure as completely as possible. In no case does such an identification imply a recommendation or endorsement by NIST, nor does it imply that the materials, equipment, or instrument identified are necessarily the best available for the purpose.

Preparation of stBLMs for SPR—Glass slides (3 × 1 × 1 mm; Fisher) were cleaned using sulfuric acid with Nochromix additive and thoroughly rinsed with Millipore water. The silicon wafers were then coated with chromium (2 nm) and gold (45 nm) using magnetron sputtering (ATC Orion; AJA International). Self-assembled monolayers (SAMs) were prepared by overnight incubation of the gold-coated slides in a 0.2 mM (M = mol/liter) ethanolic solution of the lipid tether compound HC18 (Z20-(*Z*-octadec-9-enyloxy)-3,6,9,12,15,18,22-heptaoxatetracont-31-ene-1-thiol)) (27) and β-mercaptoethanol at a 3:7 molar ratio. POPC and POPS were dissolved in ethanol and in a methanol/chloroform/water mixture (95:3:2), respectively, to yield 10 mg/ml stock solutions. Desired phospholipids mixtures were then made from these stocks. The SAM-covered slides were incubated with lipid solution for 5 min, and stBLMs were completed by rapid solvent exchange (37).

Preparation of Lipid Vesicles for Bromine Quenching and CD Experiments—Lipid vesicles were prepared as described previously (38). For Trp penetration depth experiments, brominated phosphatidylcholine lipids (Br_{6-7}, Br_{9-10}, and Br_{11-12}) were added to a final concentration of 30% while maintaining an overall 1:1 molar ratio of phosphatidylserine and phosphatidylcholine. Vesicle size (hydrodynamic radius ~45 nm) was characterized by dynamic light scattering measurements at 25 °C using 5× diluted lipid sample (~0.6 mM) on a Dynapro NanoStar (Wyatt) equipped with a 661-nm laser and Dynamics version 7.0.2 software. Autoattenuation of laser power was used to obtain optimal intensity counts of 1×10^6. Ten acquisitions with 5-s acquisition time were collected. Correlation time and peak cut-off ranges are $1.5–6.0 \times 10^4$ μs and 0.5–10,000.0 nm, respectively. Cumulant fit was applied to the autocorrelation curve to obtain the average hydrodynamic radius using a sphere model. Vesicle size distribution was extracted from the regularization fit using the Rayleigh sphere model (full width at half-maximum ~60 nm). All buffers were filtered through 0.22-μm filters (Millipore).

Preparation of stBLMs for Neutron Reflectometry—Sparsely tethered bilayer membranes were prepared as described previously with minor modifications (37). Vesicles (25 mg/ml) of the desired lipid composition were prepared by resuspending dried lipid films in aqueous pH 5.5 buffer containing 50 mM MES and 500 mM NaCl. The suspension was sonicated for 1 h in a bath sonicator and extruded at least 30 times through a 100-nm polycarbonate membrane using an extrusion kit (Avanti Polar Lipids). stBLMs were then formed by incubating the SAM with vesicle solutions for 1 h at room temperature. Non-fused vesicles were rinsed off with aqueous pH 5.5 buffer containing 50 mM MES and 25 mM NaCl.

Protein Expression and Sample Preparation—To produce uniformly deuterated wild-type α-syn, *Escherichia coli* BL21-(DE3)pLysS cells were first grown overnight at 37 °C in a starter culture (1 ml of Luria broth) inoculated with a freshly transformed single colony. The resulting cells were then used to inoculate 20 ml of H_2O-based minimal medium (39) overnight at 30 °C. Finally, 1 liter of D_2O-based minimal medium supplemented with deuterated glucose (1 g/liter) and deuterated Celtone (3 g/liter) (Cambridge Isotope Laboratories, Inc.) was then inoculated and grown overnight at 30 °C. Cells were then transferred (250 ml into 2.5 liters) and grown to an OD of ~2 and induced with isopropyl 1-thio-β-D-galactopyranoside (1 mM) for 6 h. Protein was purified as previously described (40). A calculated deuteration yield of ~98.9% was obtained from mass spectrometric analysis (15,233 Da in H_2O). Taliglucerase α (recombinant GCase) was obtained from Protalix Biotherapeutics Corp. (Carmiel, Israel). Samples were prepared in appropriate buffer (50 mM MES, 25 mM NaCl, pH 5.5), buffer-exchanged, and concentrated to the desired concentration using Amicon Ultra YM3 and YM30 centrifugal filters (Millipore) for α-syn and GCase, respectively.

GCase Activity—Experiments were performed as described previously (19).

GCase Membrane Binding Characterization—stBLMs formed on gold-coated microscopy glass slides were mounted on a custom-made surface plasmon resonance (SPR) instrument (SPR Biosystems, Germantown, MD) in the Kretschmann configuration (30). Bilayer completeness was characterized by electrochemical impedance spectroscopy and ensured to be >99%. Before the protein addition, the SPR resonance angle of the neat bilayer was monitored over time to obtain a stable baseline. Shifts in the resonance were used to quantify protein binding to the stBLM after injection of increasing concentrations of protein into the sample chamber. The system was allowed to equilibrate for 30 min before each subsequent protein addition at 20 °C.

Trp fluorescence was measured (λ_{ex} = 295 nm, λ_{obs} = 300–500 nm, 0.3-s integration time, 1-nm slits, 25 °C) in a microquartz cuvette with 3-mm path length (Starna Cells, working volume = 120 μl) using a Fluorolog 3 spectrofluorometer (Horiba Jobin Yvon) in the absence and presence (30 mol %) of brominated POPC lipids in POPC/POPS vesicles. Experiments were performed for 300 nM and 1 μM GCase in 50 mM MES, 25 mM NaCl buffer, pH 5.5, and at a lipid/protein molar ratio of 350. Although variations in the absolute amount of quenching are observed, the trend relative to the three bromine positions is consistent and reproducible.

CD measurements (198–260 nm, 1-nm steps, 1-nm bandwidth, 1-s integration time, 100 nm/min, 25 °C) were performed in 1-mm quartz cuvettes using a Jasco J-715 spectropolarimeter (Jasco Analytical Instruments). An average of two scans (three accumulations each) is reported with buffer backgrounds subtracted.

Neutron Reflectometry—NR measurements were performed at the NG7 and NGD-MAGIK reflectometers at the NIST Center for Neutron Research (NCNR) (41). Reflectivity curves were recorded for momentum transfer values $0 \leq q_z \leq 0.25$ Å^{-1}. stBLMs were prepared on SAM-coated 3-inch diameter silicon wafers assembled in an NCNR reflectometry flow cell (42). Every subsequent condition of the stBLM was measured using at least two isotopically different bulk solvents (contrasts) (*i.e.* aqueous buffer prepared from D_2O and H_2O). For each measured contrast, adequate counting statistics were obtained after 5–7 h. The flow cell allows for *in situ* buffer exchange; therefore, subsequent measurements were performed on the same sample area. The flow cell was maintained at room temperature. In order to minimize nonspecific binding, measurements of the stBLM with GCase (300 nM) alone were made after a short incubation period (20 min) followed by a rinse step. For measurements with α-syn (300 nM), a rinse step was avoided because its membrane binding is highly dynamic, and thus stBLM was incubated with the protein solution during the entire measurement time.

Data Analysis—SPR equilibrium response (R_{eq}) data were modeled by a Langmuir adsorption model (30),

$$R_{eq} = \frac{pB_{max}}{p + K_d} \quad \text{(Eq. 1)}$$

where p is the concentration of GCase, K_d is the equilibrium dissociation constant, and B_{max} is the saturation value of the SPR response at $p \to \infty$. Data fitting was performed using IGOR Pro 6.32A (Wavemetrics).

Trp mean depth (h_m) was obtained using the following equation (43),

$$\ln \frac{F_0}{F} = \frac{S}{\sigma\sqrt{2\pi}} \exp\left(-\frac{(h - h_m)^2}{2\sigma^2}\right) \quad \text{(Eq. 2)}$$

where F_0 and F are the Trp fluorescence intensities measured in the absence and presence of bromine; h is the distance from the bilayer center; and the fitting parameters, σ and S, are the dispersion and area, respectively. Data fitting was performed using IGOR Pro 6.32A (Wavemetrics).

The one-dimensional structural profile along the lipid bilayer normal was obtained from NR using a hybrid of a stratified slab model for the solid substrate (44), a continuous distribution model for the stBLM (45), and a monotonic Hermite spline for the model-free envelope of the protein (28). Individual slabs were implemented for the bulk silicon, the silicon oxide, the chromium, and the gold layers. Fit parameters are thickness and neutron scattering length density for each layer (Table 1), except for the bulk silicon. One global roughness parameter applies to all substrate interfaces. Individual submolecular groups implemented in the continuous distribution model are β-mercaptoethanol, tether PEG chains, tether glycerol groups, substrate-proximal and substrate-distal phosphatidylcholine and phosphatidylserine headgroups, substrate-proximal and substrate-distal methylene, and methyl chains of lipid and tether molecules. Fit parameters are the bilayer hydrocarbon thickness for each bilayer leaflet, bilayer completeness, tether surface density, tether thickness, and β-mercaptoethanol surface density (Table 1). One roughness parameter is applied to all distributions.

The Hermite spline that describes the volume occupancy profile of the protein, VO(z), is defined by control points, which are on average 15 Å apart. The spatial extension of the protein

along the bilayer normal determines the number of control points, and it is determined iteratively during model optimization. Fit parameters for each control point are the volume occupancy of the envelope and the deviation from a position defined by equidistant control points throughout the spline. A constant neutron scattering length density (nSLD) is applied to spline functions that describe the volume occupancy of either completely protiated or deuterated protein material.

In the case of the α-syn·GCase complex that combines protiated GCase and d-α-syn, the nSLD is a function of z: nSLD(z). This variable nSLD is modeled using a monotonic Hermite spline itself, sharing the position of the control points that define the volume occupancy spline. The nSLD can vary between values for entirely protiated and deuterated material (*i.e.* GCase and d-α-syn). Volume occupancy profiles for the individual components of the complex are extracted after the fit by a linear decomposition. First, the nSLD profile is decomposed into the two contributions ($\text{frac}_{\text{syn}}(z)$, $\text{frac}_{\text{GCase}}(z)$) from the protiated component (GCase, $\text{nSLD}_{\text{GCase}} = 1.67 \times 10^{-6}$ Å^{-2}) and the deuterated component (α-syn, $\text{nSLD}_{\text{syn}} = 6.12 \times 10^{-6}$ Å^{-2}) using the equation,

$$\text{nSLD}(z) = \text{frac}_{\text{syn}}(z) \times \text{nSLD}_{\text{syn}} + \text{frac}_{\text{GCase}}(z) \times \text{nSLD}_{\text{GCase}} \quad \text{(Eq. 3)}$$

for all z: $1 = \text{frac}_{\text{syn}}(z) + \text{frac}_{\text{GCase}}(z)$.

In a second step, individual volume occupancies for the protiated and deuterated components are calculated using the following equations.

$$\text{VO}_{\text{syn}}(z) = \text{VO}(z) \times \text{frac}_{\text{syn}}(z) \quad \text{(Eq. 4)}$$

$$\text{VO}_{\text{GCase}}(z) = \text{VO}(z) \times \text{frac}_{\text{GCase}}(z) \quad \text{(Eq. 5)}$$

Data modeling that determines the orientation of a protein at the lipid bilayer requires the use of a structural model that is assumed to be invariant (rigid body modeling) (31, 33). For GCase, the Protein Data Bank structure with the identifier 1OGS (46) was augmented by adding hydrogen atoms using the MolProbity Web service (47). The protein possesses four glycosylation sites, and glycans were added to those sites choosing the most frequently occurring species (48), using the appropriately patched α-mannose, β-xylose, *N*-acetyl-D-glucosamine, and fucose subunits from the CHARMM force field (49). The structure of the attached glycans was energy-minimized using NAMD, and the glycoprotein was equilibrated via a 10-ns simulation using the generalized Born approximation for the solvent (50). The obtained structure file was used for modeling of the NR data with two continuous fit parameters, equivalent to the two Euler angles (β, γ), describing the orientation of the protein at the interface.

The orientation of Chain A in 1OGS (46) is defined as the (0°, 0°) orientation. Every other orientation (β, γ) can be obtained by extrinsic rotations of the protein around the axes of the bilayer coordinate system. First, the protein is rotated by γ about the membrane normal, or the z axis. Second, the protein is rotated by β about the x axis, which is in plane with the membrane. The third Euler angle, α, would correspond to a third extrinsic rotation around the z axis. NR is invariant to this orientation. The fit allows for orientations within $0° \leq \beta \leq 90°$ and $0° \leq \gamma < 360°$.

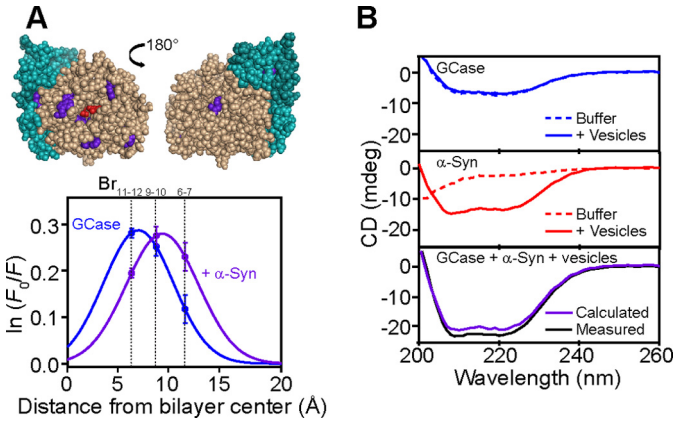

FIGURE 1. **Insertion of GCase Trp side chains into the membrane.** *A*, *top*, GCase crystal structure (Protein Data Bank code 1OGS) (46). TIM barrel motif and β-sheet domains are *colored taupe* and *teal*, respectively. Trp and active site Glu residues are *colored purple* and *red*, respectively. Eight of the 12 Trp residues have some solvent exposure. *Bottom*, steady-state Trp fluorescence of GCase (1 μM) in the presence of POPC/POPS (F_0) and POPC/POPS vesicles containing 30% brominated phosphatidylcholine lipids (F). The location of the three different bromine sites is denoted by *dotted lines*. *Solid lines*, fits to distribution analysis. *Error bars*, S.D. values ($n = 2$). *B*, CD spectroscopy was employed to measure the secondary structure of GCase alone (*top panel*), α-syn alone (*middle panel*) in solution (*dashed line*) and in the presence of POPC/POPS vesicles (*solid line*), and α-syn in the presence of GCase and POPC/POPS vesicles (*bottom panel*). Experiments were performed in pH 5.5 buffer (50 mM MES and 25 mM NaCl) with 2 μM GCase, 5 μM α-syn, and 700 μM POPC/POPS (1:1) vesicles. Mathematical summation of independently measured spectra of α-syn and GCase at the same concentrations in the presence of vesicles is also plotted (*bottom panel*). Averages of independently measured spectra ($n = 2$) are shown.

Data modeling and optimization of model parameters was performed using the ga_refl and Refl1D software packages developed at the NCNR (42). Optimization of model parameters is achieved either by the combined use of a genetic algorithm, a simplex amoeba algorithm for efficient searching of parameter space, and a Levenberg-Marquardt non-linear least square algorithm to refine the fit, or by using a differential evolution Markov chain. All reflectivity curves of one data set were fit simultaneously to the same model, sharing fit parameters, for example, for the solid substrate. Either a Monte Carlo simulation (26) or the statistical analysis of the Monte Carlo Markov chain (42) was used to determine the median model parameter values and their 68% confidence limits. Both methods deliver a bias-free and objective estimate of parameter uncertainties and, in this way, avoid overparameterization of the model.

The model structures of the membrane-associated α-syn·GCase complex were based on the secondary structure of micelle-bound α-syn (51) and the x-ray structure of GCase (46), combined with the previously generated model of the α-syn·GCase complex in solution (18). The structures were generated with the Maestro and Prime programs (Schrödinger, Inc.).

RESULTS

Effect of α-Synuclein on GCase Membrane Binding Probed by Trp Fluorescence and Circular Dichroism Spectroscopy—GCase contains 12 intrinsic Trp residues located within its hydrophobic interior and in solvent-accessible loops (Fig. 1*A*, *top*). To

determine whether membrane association of GCase is modulated by α-syn, we measured the steady-state Trp fluorescence of GCase upon binding to phospholipid vesicles containing the heavy atom, collisional quencher bromine, which allows the determination of Trp side chain penetration depth (Fig. 1*A*, *bottom*). α-Syn does not contain any native Trp residues and thus does not contribute to the measured intensities. Three independent bromine positions (Br_{6-7}, Br_{9-10}, and Br_{11-12}) served as markers for 11, 8.3, and 6 Å from the bilayer center (52). Equimolar phosphatidylcholine and phosphatidylserine (POPC/POPS) vesicles contained either none or one of the three different brominated lipids (30 mol %). The logarithm of the ratio of Trp fluorescence intensities measured in the absence (F_0) and presence of bromine (F) is plotted *versus* depth (43). Trp fluorescence quenching for GCase alone is observed for all sites, with Br_{11-12} exhibiting the greatest effect, indicating that at least one or more of the Trp residues is partitioning into the hydrocarbon acyl chains, with a mean depth (h_m) of 6.6 ± 0.7 Å from bilayer center, consistent with prior work using nitroxide spin-labeled lipids as quenchers (53). A marked difference is observed upon the addition of α-syn. Trp quenching is increased by Br_{6-7} with a concomitant decrease by Br_{11-12}, suggesting that α-syn lifts GCase up toward (~2.3 Å) the lipid-water interface. A membrane-binding, N-terminal α-syn peptide (residues 1–19) had no effect on the GCase penetration depth, showing that perturbations of GCase membrane insertion only occur with full-length protein (data not shown).

To gain insights into whether this observed Trp displacement event is coupled to a structural rearrangement of the enzyme, we employed CD spectroscopy to probe for the changes in secondary structure content. The measured CD spectra are indistinguishable for GCase alone in buffer and in the presence of POPC/POPS vesicles, indicating the preservation of its folded structure on the membrane (Fig. 1*B*, *top*). Thus, the CD results require that any conformational changes that involve the insertion of Trp residues upon membrane binding must involve no net change of enzyme secondary structure.

For the complex with α-syn, however, the CD spectrum reveals a small increase in helical content when compared with the sum of the spectra of the individual proteins (Fig. 1*B*, *bottom*). Although it is not discernible whether the increased CD signal is solely attributable to GCase or α-syn or both, we postulate that it is more likely to be due to α-syn because it is known to be conformationally labile (4) and undergoes folding from disordered to helical structure in the presence of phospholipids (Fig. 1*B*, *middle*). Under this assumption, the change in secondary structure would be a modest ~5% increase in α-helicity, only seven additional helical residues. Based on the data, we suggest that GCase interaction with α-syn results in a shallower penetration depth of the enzyme on the bilayer with minimal change to its folded structure.

GCase Membrane Interaction and Structural Orientation Determined by Neutron Reflectivity—To obtain structural information on how GCase interacts with α-syn on a membrane, we first needed to measure neutron reflection of GCase on a POPC/POPS stBLM and determine its binding orientation. Membrane binding and binding affinity of GCase with POPC/POPS stBLM were confirmed and assessed by SPR spectroscopy (Fig. 2). As expected, the relative membrane binding affinities correlate with GCase activity, with a strong preference for negatively charged phosphatidylserine lipids, confirming that the enzyme-lipid interaction is vital for catalysis (Fig. 2, *inset*).

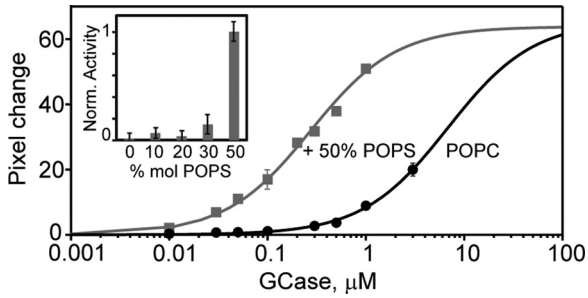

FIGURE 2. **Effect of POPS on GCase membrane association and activity.** GCase binding to POPC (*circles*) and equimolar POPC/POPS (*squares*) stBLMs is quantified by SPR spectroscopy. One pixel change corresponds to a SPR minimum angle change of 0.0067°. *Solid lines*, fits to a Langmuir adsorption process (equilibrium dissociation constants (K_d) are 210 ± 6 nM and 6.8 ± 1.7 μM for POPC/POPS and POPC, respectively). *Error bars*, SPR signal variations at the plateau of each addition. *Inset*, normalized GCase activity measured in vesicles containing different amounts of POPS (0–50%). *Error bars*, S.D. values ($n = 2$).

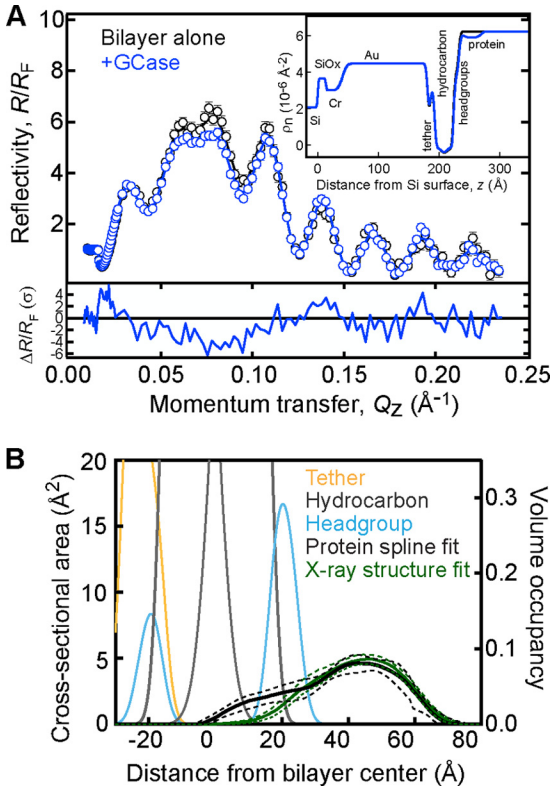

FIGURE 3. **GCase membrane binding probed by neutron reflectometry.** *A*, neutron reflectivity (R/R_F) for a POPC/POPS stBLM and changes resulting from the addition of GCase (300 nM) in D_2O. *Error bars*, 68% confidence intervals for the measured reflectivity based on Poisson statistics. The differences between R/R_F curves ($\Delta R/R_F$) are shown in units normalized to the S.D. value (σ) of the experimental error. Spline model fits to the data are shown as *solid lines*. Best fit neutron scattering length density profiles for all four measurements calculated from the composition-space model are shown in the *inset*. *B*, simplified molecular distributions for each organic interface layer of the POPC/POPS stBLM and GCase obtained from the best fit of reflectivity data to the spline fit model. The median protein envelope is shown with its associated 68% confidence intervals (*black*). Volume occupancy is indicated on the *right axis*. Comparison of the median orientation fit using a structural model of glycosylated GCase is shown with 68% confidence intervals (*green*). See Table 1 for parameters.

TABLE 1

Median model parameter values and 68% confidence intervals for POPC/POPS stBLMs in the presence of GCase and α-synuclein

Parameters for the neat bilayer that were determined simultaneously are omitted.

Fit parameters	GCase[a]	GCase[b]	GCase and d-α-syn	d-α-syn
Substrate				
SiO_2	$d^c = 13.3 \pm 3.0$ Å $\rho^d = 3.66 \pm 0.11 \times 10^{-6}$ Å^{-2}	$d = 11.1 \pm 0.9$ Å $\rho = 3.75 \pm 0.05 \times 10^{-6}$ Å^{-2}	$d = 8.1 \pm 0.7$ Å $\rho = 3.55 \times 10^{-6}$ Å^{-2} (fixed)	$d = 24.2 \pm 0.7$ Å $\rho = 3.50 \pm 0.20 \times 10^{-6}$ Å^{-2}
Chromium	$d = 27.1 \pm 2.9$ Å $\rho = 3.00 \pm 0.07 \times 10^{-6}$ Å^{-2}	$d = 29.4 \pm 0.8$ Å $\rho = 3.06 \pm 0.02 \times 10^{-6}$ Å^{-2}	$d = 42.6 \pm 0.9$ Å $\rho = 3.01 \pm 0.02 \times 10^{-6}$ Å^{-2}	$d = 18.5 \pm 0.8$ Å $\rho = 2.83 \pm 0.05 \times 10^{-6}$ Å^{-2}
Gold	$d = 141.1 \pm 0.9$ Å $\rho = 4.48 \pm 0.04\ 10^{-6}$ Å^{-2}	$d = 140.2 \pm 0.3$ Å $\rho = 4.47 \pm 0.02\ 10^{-6}$ Å^{-2}	$d = 122.8 \pm 0.4$ Å $\rho = 4.55 \pm 0.02 \times 10^{-6}$ Å^{-2}	$d = 156.2 \pm 0.5$ Å $\rho = 4.52 \pm 0.02 \times 10^{-6}$ Å^{-2}
Lipid bilayer				
Tether	$d = 11.2 \pm 0.2$ Å $\chi^e = 0.41 \pm 0.25$ $n^f = 3.1 \pm 1.4$	$d = 11.3 \pm 0.2$ Å $\chi = 0.81 \pm 0.25$ $n = 3.0 \pm 1.3$	$d = 10.9 \pm 0.2$ Å $\chi = 0.47 \pm 0.26$ $n = 3.3 \pm 0.8$	$d = 11.5 \pm 0.1$ Å $\chi = 0.52 \pm 0.06$ $n = 3.4 \pm 0.6$
Proximal lipid leaflet (Å)	$d = 16.1 \pm 0.8$ Å	$d = 14.8 \pm 0.5$ Å	$d = 15.7 \pm 0.6$ Å	$d = 15.9 \pm 0.3$ Å
Distal lipid leaflet (Å)	$d = 16.1 \pm 0.4$ Å	$d = 16.5 \pm 0.5$ Å	$d = 13.9 \pm 0.4$ Å	$d = 14.5 \pm 0.4$ Å
Thickness change per leaflet from neat bilayer (Å)	0.3 ± 0.1 Å	0.1 ± 0.1 Å	-0.1 ± 0.2 Å	0.5 ± 0.1 Å
Area per lipid (Å^2)	57.6 ± 1.4 Å^2	56.0 ± 1.2 Å^2	66.5 ± 2.0 Å^2	64.0 ± 0.9 Å^2
Bilayer completeness	1.00 ± 0.01	1.00 ± 0.01	1.00 ± 0.01	1.00 ± 0.01
Protein				
Volume surface density (Å^3/Å^2)	3.3 ± 0.4 (47 ± 6 ng/cm^2)	3.1 ± 0.3 (44 ± 5 ng/cm^2)	12.4 ± 1.5 (177 ± 22 ng/cm^2)	3.1 ± 0.4 (44 ± 6 ng/cm^2)

[a] Spline fit.
[b] Orientation fit.
[c] Thickness of the layer.
[d] Neutron scattering length density.
[e] Molar fraction in proximal lipid leaflet.
[f] Number of β-mercaptoethanol molecules per tether.

Two reflectivity curves were measured using either H_2O- or D_2O-based buffer for the stBLM alone and the stBLM after GCase incubation, respectively. Representative D_2O data are shown in Fig. 3*A* (Table 1). All measurements were evaluated using a global fit to obtain a structural profile of the stBLM and of the enzyme at the membrane interface (28, 31). The resulting bilayer structure and median protein envelope yield an excellent fit to the measured reflectivity (Fig. 3*B*).

The protein envelope from the free form spline model indicates that GCase is peripherally associated with a peak density at a distance of 50 Å from the bilayer center, with the majority of GCase density in the aqueous surrounding. In accord with the Trp penetration result (Fig. 1*A*), a portion of the enzyme interacts within the phospholipid headgroups and penetrates into the acyl chain region of the outer leaflet. Using previously established rigid body modeling methods (28, 31) and a Monte Carlo Markov chain data refinement algorithm (42), the spatial association and orientation of glycosylated GCase on the stBLM is obtained based on the GCase x-ray crystal structure (Protein Data Bank code 1OGS) (46). Within the 68% probability bounds (Fig. 4*A*), the majority of orientations are quite similar (Fig. 4*B*), with only modest variation in the Euler rotation angles of β and γ. A comparison of the free form spline envelope (*black curve*) and the envelope from the orientation fit (*green curve*) for values of $\beta \leq 90°$ is shown in Fig. 3*B*. The profiles that are outside the lipid membrane are nearly indistinguishable, suggesting that the globular fold of soluble GCase is preserved upon membrane association, consistent with the CD data (Fig. 1*B*). An example orientation (20°, 90°) is shown in Fig. 4*C*. GCase has a $(\alpha/\beta)_8$ TIM barrel (Fig. 4*C*, *taupe*), which contains the two catalytic glutamic acids (*red*) and two flanking β-sheet domains (Fig. 4*C*, *cyan*). Of the probable orientations, this orientation best balances interactions between the glycans and the lipid headgroups with accessibility of the catalytic active site to the membrane.

The spline fit for GCase density shows greater density penetrating more deeply into the outer lipid leaflet compared with the orientation fit based on the crystal structure (Fig. 3*B*). From the orientation fit, the putative membrane interface (Fig. 4*D*) suggests that flexible loops 2 and 3 could insert into the bilayer, resulting in the penetration of Trp-348 and Trp-393 into the acyl hydrocarbon chains, as observed by fluorescence measurements. It is plausible that in order to accommodate side chain/peptide penetration, lipid reorganization also occurs, which could contribute to differences in the density profiles. Consistent with this view, a cluster of bound sulfate ions is seen interacting with loop 2 in the x-ray crystal structure, hinting that loop 2 might interact with phosphate headgroups of the membrane (54). Additional experimental support was obtained using a synthetic peptide consisting of the loop 2 sequence (Ac-GSKFWEQSVR-NH_2) to show that it has an affinity for POPC/POPS vesicles (data not shown). In contrast, the corresponding loop 3 peptide (Ac-EGGPNWVRNFVD-NH_2) did not interact with the membrane based on Trp fluorescence (data not shown), but this result does not preclude GCase-membrane interactions that include the loop 3 Trp.

α-Syn-GCase Interaction on the Membrane Probed by Neutron Reflectivity—The use of deuterated α-syn and protiated GCase facilitated extraction of the density profiles for each protein in the membrane-bound complex (Fig. 5). From these fits, there is an approximate 1.0:1.2 molar ratio of d-α-syn and GCase at the membrane, consistent with the presence of 1:1 complex as determined previously (19). The extracted profile for GCase from the complex is in agreement with that obtained for GCase alone (*i.e.* the majority of the density is peripheral to the membrane, and a portion penetrates into the outer leaflet) (Fig. 5*B*), suggesting that GCase maintains a similar orientation in the complex. Interestingly, the mean of the penetration of GCase in α-syn·GCase complex does appear somewhat smaller than for free GCase but remains within 68% confidence limits (Fig. 5*B*).

The overall volume occupancy with the complex is about twice as large compared with data collected for GCase alone, reaching a maximum of 25% at 40 Å from the bilayer center.

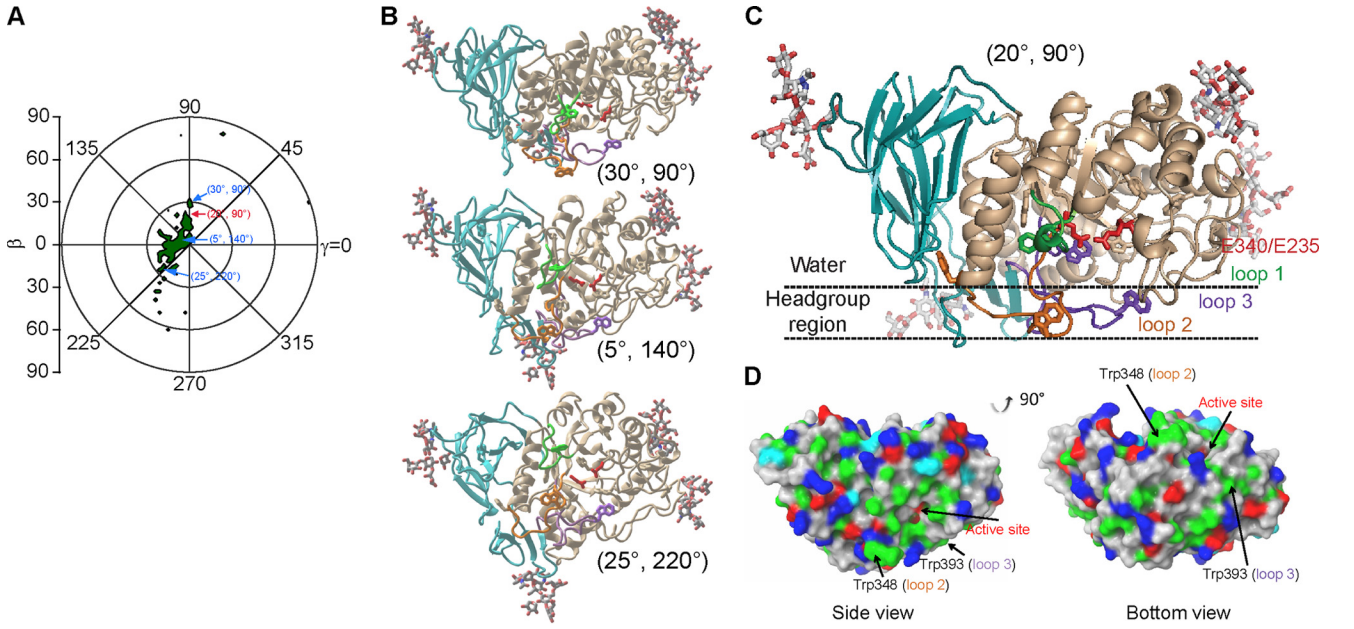

FIGURE 4. **Structure of GCase at the membrane interface revealed by neutron reflectometry.** *A*, probability plot for the orientation of GCase at the membrane obtained from rigid body modeling using a structural model of glycosylated GCase as a function of the Euler angles (β, γ). The contour represents a confidence limit of 68%. Protein orientation is sufficiently described by two of three Euler angles, β and γ. Any orientation is achieved first rotating by γ about the *z* axis (membrane normal) and second by β about the *x* axis (in the plane of the membrane). The third Euler angle, α, does not affect the NR profile along *z* because it constitutes a final rotation of the sample about the membrane normal. Here, we have defined (β, $\gamma = 0°, 0°$) as the orientation of Protein Data Bank file 1OGS (chain A) (46) with the *z* coordinate axis taken as the normal to the membrane surface. Euler angles for the structures shown in Fig. 4*B* are indicated in *blue* and that for Fig. 4*C* is shown in *red*. *B*, molecular structures of probable orientations of GCase at the membrane interface. The TIM barrel motif and β-sheet domains are *colored taupe* and *teal*, respectively. Catalytic Glu residues, 235 and 340, are red. The flexible loops near the active site are loop 1 (*green*; residues 311–319), loop 2 (*orange*; residues 341–357), and loop 3 (*purple*; residues 380–402) and are as indicated. Trp residues and glycosylation sites (Asn-19, Asn-59, Asn-146, and Asn-270) (48) are also shown. *C*, *expanded view* of the molecular structure with probable orientation ($\beta = 20°$, $\gamma = 90°$) of GCase at the membrane interface. The TIM barrel motif and β-sheet domains are *colored taupe* and *teal*, respectively. Catalytic Glu residues, 235 and 340, and flexible loops 1–3 near the active site are indicated, *colored* as in Fig. 4*B*, with Trp residues and glycosylation sites also shown. *D*, molecular surface for GCase. The (20°, 90°) orientation, the same as in Fig. 4*C*, is shown in the *left panel* (side view). In the *right panel*, the membrane-facing view of GCase (*bottom view*, rotated 90° from the *left panel*) is shown. The surface is *colored blue* for lysine and arginine residues, *cyan* for histidine, *red* for aspartate and glutamate, and *green* for side chains of hydrophobic residues (alanine, valine, leucine, isoleucine, methionine, phenylalanine, and tryptophan). The enzyme active site cavity is indicated as well as the tryptophan residues of loops 2 and 3.

This level of coverage implies relatively close packing, with on average 20–30 Å of unoccupied membrane lying between a protein complex and its nearest neighbor; thus, nonspecific steric contacts are possible. An additional small amount of protein density (1–7% volume occupancy) extending beyond 80 Å is also observed, which we attribute to the presence of nonspecifically associated, oligomerized, or aggregated proteins due to the longer incubation time (~5–7 h) in these experiments. Similar features were observed for NR data collected for GCase alone under comparable conditions.

Striking differences are observed between the structural envelopes extracted for d-α-syn in the complex (Fig. 5*C*, *green*) compared with that collected for d-α-syn alone (Fig. 5*C*, *red*). Clearly, interaction of d-α-syn with the bilayer is perturbed in the presence of GCase (Fig. 5, *C* and *D*). This new insight is not evident from any other data and is only revealed through NR measurements. Unlike the protein alone, the structural envelope of α-syn in the complex is redistributed, exhibiting a second peak at about 50 Å from the bilayer center, evidence for an interaction of α-syn and GCase beyond the membrane surface (Fig. 5*C*). The observed changes cannot simply be due to crowding at the membrane surface; α-syn in the absence of GCase has been measured at comparable membrane coverage, and no changes have been observed resembling those seen for the complex (34). Unfortunately, we are near the limit of detection by NR, so lowering protein concentrations of α-syn and GCase below 300 nM is not feasible at this time; therefore, it is uncertain to what extent steric contacts might be perturbing the NR results.

Integration of these profiles shows that ~48 residues as compared with ~73 residues of d-α-syn are embedded in the membrane in the presence and absence of GCase, respectively (Fig. 5*D*). The α-syn alone data are fully supported by other structural studies where the N-terminal region up to around residue 95 is membrane-associated (4) and consistent with previous NR work on protiated α-syn (34). Recall that the CD spectra of membrane-bound α-syn and GCase indicated that α-syn maintains or possibly slightly increases its helical content (Fig. 1*B*). The implication is that α-syn retains its membrane-associated helical structure in the presence of membrane-bound GCase, yet the NR data suggest that roughly half of the α-helical structure lies above the plane of the bilayer. Such a situation has never before been observed for membrane-bound α-syn (4); all previous studies are consistent with the entire helical region being membrane-associated. However, the NR data cannot rule out the possibility that some portion of α-syn sitting above the bilayer plane still retains some contact with lipid molecules.

DISCUSSION

The work here shows that GCase binds to and partially inserts into the POPC/POPS membrane, involving structural reorganization of GCase loops at the membrane interface that extend into the hydrocarbon tail region of the membrane. The

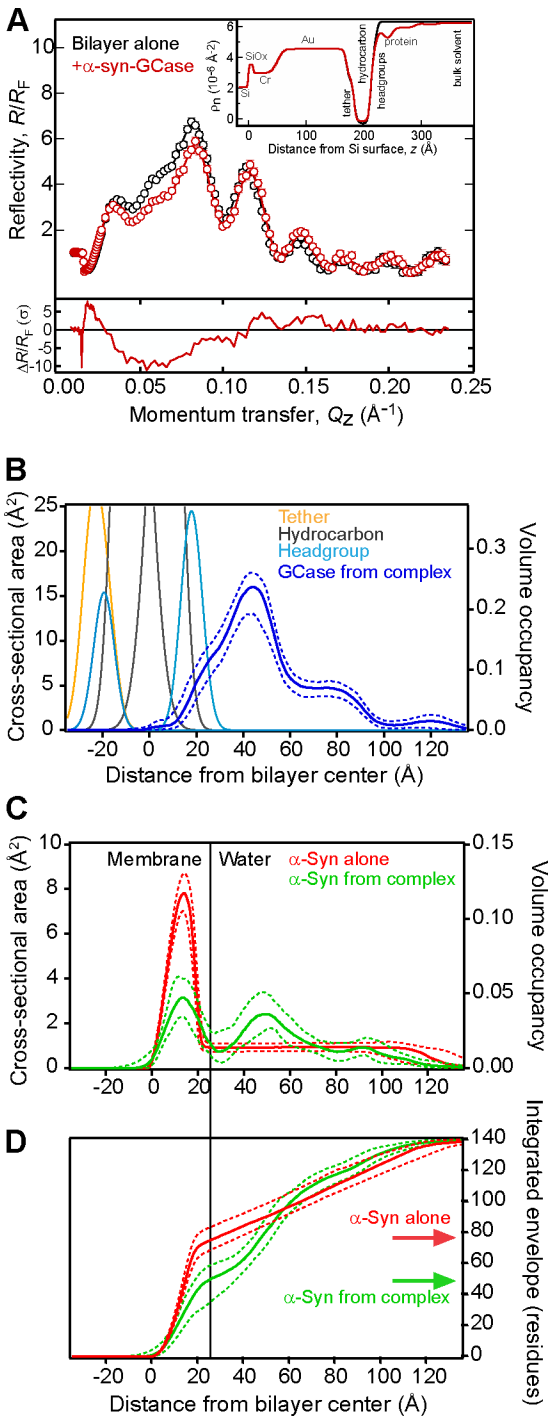

FIGURE 5. **Interaction of GCase and deuterated α-syn on the membrane probed by neutron reflectometry.** *A*, neutron reflectivity (R/R_F) for a POPC/POPS stBLM and changes resulting from the addition of GCase and d-α-syn (300 nM each) in D_2O. *Error bars*, 68% confidence intervals for the measured reflectivity based on Poisson statistics. The differences between R/R_F curves ($\Delta R/R_F$) are shown in units normalized to the S.D. (σ) of the experimental error. Spline model fits to the data are shown as *solid lines*. Best fit neutron scattering length density profiles for all four measurements calculated from the composition-space model are shown in the *inset*. *B*, simplified molecular distributions for each organic interface layer of the POPC/POPS stBLM and the median protein envelope for protiated GCase obtained from the best fit of reflectivity data to the spline fit model. *Dashed lines*, 68% confidence intervals. Volume occupancy is indicated on the *right axis*. See Table 1 for parameters. *C*, median protein envelope attributable to d-α-syn (*green*) is shown. For comparison, the median protein envelope obtained from fits to NR of d-α-syn in the absence of GCase (300 nM; *red*) on POPC/POPS stBLM is also shown. *Dashed lines* represent 68% confidence intervals. Volume occupancy is indicated on the *right axis*. See Table 1 for parameters. *D*, the integrated profiles for d-α-syn alone (*red*) and d-α-syn extracted from α-syn·GCase complex (*green*) are shown. The integral is normalized to the total number of residues (140 residues). *Dashed lines* represent 68% confidence intervals.

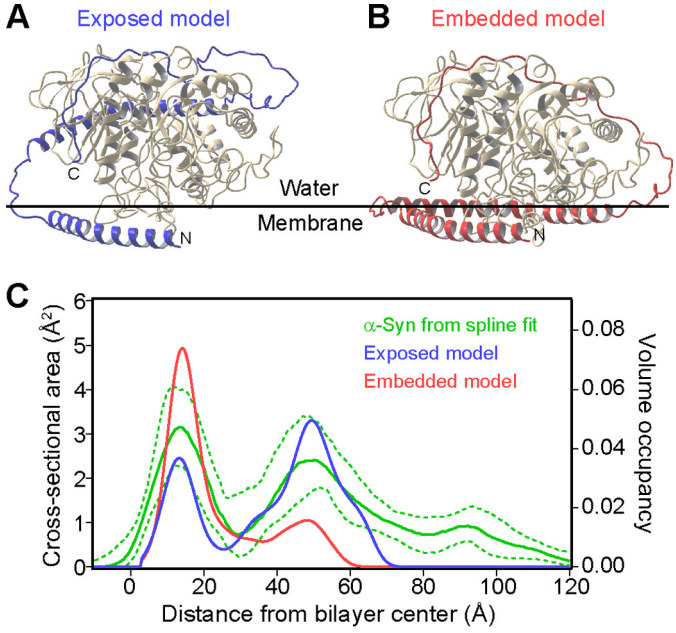

FIGURE 6. **Model structures of the membrane-bound α-syn·GCase complex.** GCase is shown in *gray* and α-syn in *blue* and *red* for the exposed (*A*) and embedded model (*B*), respectively. The α-syn N and C termini are labeled. The *viewpoint* corresponds to a rotation of 60° about the membrane normal of Fig. 4*C*. *C*, comparison between the predicted cross-sectional profiles for α-syn in the two α-syn·GCase models (*A* and *B*) and the spline fit extracted from the α-syn·GCase NR data (reproduced from Fig. 5*C*). *Dashed lines* represent 68% confidence intervals. Volume occupancy is indicated on the *right axis*.

entrance to the active site for the most probable orientations (Fig. 4, *C* and *D*) does not directly face the plane of the bilayer. Instead, the entrance lies just above the membrane-water interface, where it presumably remains lipid-accessible and, therefore, catalytically competent. Sap C, the enzymatic cofactor of GCase (13, 14), has been proposed to interact with GCase at a site near the active site entrance (55), in a cleft that lies to the left of the entrance, as seen in Fig. 4*C*. This proposed interaction site is solvent-accessible and lies adjacent to the membrane. The positioning of this site helps to explain how Sap C can bind GCase both in the presence and absence of membrane (22) and suggests that its enhancement of GCase activity probably involves direct interaction with both GCase and the membrane, as proposed previously (56).

The addition of GCase has a profound effect on the NR profile for α-syn, causing most of its embedded helical region to move above the plane of the membrane. To visualize how the membrane-associated α-syn·GCase complex might look, a model structure was generated based on micelle-bound α-syn (51). In this structure, the N-terminal region is composed of two α-helices consisting of residues 3–37 and 45–92. The first helical region, known to be most important for membrane binding (34, 40, 57–59), is embedded in the membrane in the model, whereas the second helix is positioned above the membrane and in contact with GCase (Fig. 6*A*, *Exposed model*). The remaining C-terminal tail region was modeled based on the

solution α-syn·GCase complex (18). The cross-sectional profile calculated based on this model shows good agreement with that generated from the NR experiment, in particular, reproducing two of the three peaks, positioned at 13 and 50 Å from the bilayer center (Fig. 6*C*). This model is in accord with prior Förster resonance energy transfer fluorescence data, where it was shown that residues 57, 100, and 136 directly interact with GCase, whereas residues 7 and 40 are in close proximity to GCase and in direct contact with the bilayer (19).

Of course, our earlier fluorescence data (19) and the current NR results do not reveal exactly where on the GCase surface the α-syn helices make contact; such details must await future studies.

For comparison, the profile for a model structure with all helical residues fully embedded (Fig. 6*B*, *Embedded model*) is also shown (Fig. 6*C*). The embedded model profile has a higher peak at 14 Å, similar to membrane-bound α-syn alone (Fig. 5*C*), and a much smaller one at 48 Å. Neither model produced the third peak in the profile at roughly 90 Å. This peak probably arises from α-syn interacting with a small population of GCase multimer or aggregate at the membrane, the presence of which is implicated in the NR profile for GCase (Fig. 5*B*). Interestingly, the α-syn NR profile peak magnitudes lie between those of the exposed and embedded model profiles, suggesting that the complex structure might be an intermediate between the two models or that they are in dynamic equilibrium. This movement probably exposes amyloidogenic core residues of α-syn (residues 30–100), increasing their accessibility to lysosomal proteases, and thus could play some role in PD etiology. Because the dissociation constant for complex formation is in the micromolar range (19), we expect that there is also some contribution from free membrane-bound α-syn at the concentrations used in this study (0.3 μM). Nevertheless, the data corroborate our previous suggestion that on the membrane surface, the α-syn-GCase interaction involves a larger α-syn region compared with that found in solution (19).

Although the addition of α-syn has no significant effect on GCase secondary structure or its orientation relative to the membrane, it does shift GCase away a small distance from the membrane. Previously, it was suggested that inhibition by α-syn might be due to hindered substrate entry into the active site as well as release of product. The results here suggest an additional possibility, that displacement of GCase makes the active site too far from the bilayer for optimal substrate access. However, other explanations cannot be excluded, such as subtle alterations in the active site configuration as well as orientation of nearby loops.

In conclusion, using neutron reflectometry, we have structurally characterized a challenging system, namely the formation of a protein complex on the membrane, revealing features not obtainable by other techniques. Future work on how lysosomal degradation of α-syn is affected by GCase interaction and how Sap C reverses GCase inhibition by α-syn should provide additional insight into the mechanistic link between α-syn and GCase in PD.

Acknowledgments—The recombinant GCase used was a gift from Protalix Biotherapeutics (Carmiel, Israel). We thank the NHLBI, National Institutes of Health, Biophysics and Biochemistry Cores for the use of equipment and technical expertise.

REFERENCES

1. Hardy, J., Cai, H., Cookson, M. R., Gwinn-Hardy, K., and Singleton, A. (2006) Genetics of Parkinson's disease and parkinsonism. *Ann. Neurol.* **60,** 389–398
2. Lesage, S., Anheim, M., Letournel, F., Bousset, L., Honoré, A., Rozas, N., Pieri, L., Madiona, K., Dürr, A., Melki, R., Verny, C., Brice, A., and French Parkinson's Disease Genetics Study Group (2013) G51D α-synuclein mutation causes a novel parkinsonian-pyramidal syndrome. *Ann. Neurol.* **73,** 459–471
3. Proukakis, C., Dudzik, C. G., Brier, T., MacKay, D. S., Cooper, J. M., Millhauser, G. L., Houlden, H., and Schapira, A. H. (2013) A novel α-synuclein missense mutation in Parkinson disease. *Neurology* **80,** 1062–1064
4. Pfefferkorn, C. M., Jiang, Z., and Lee, J. C. (2012) Biophysics of α-synuclein membrane interactions. *Biochim. Biophys. Acta* **1818,** 162–171
5. Lashuel, H. A., Overk, C. R., Oueslati, A., and Masliah, E. (2013) The many faces of α-synuclein: from structure and toxicity to therapeutic target. *Nat. Rev. Neurosci.* **14,** 38–48
6. Goker-Alpan, O., Stubblefield, B. K., Giasson, B. I., and Sidransky, E. (2010) Glucocerebrosidase is present in α-synuclein inclusions in Lewy body disorders. *Acta Neuropathol.* **120,** 641–649
7. Choi, J. H., Stubblefield, B., Cookson, M. R., Goldin, E., Velayati, A., Tayebi, N., and Sidransky, E. (2011) Aggregation of α-synuclein in brain samples from subjects with glucocerebrosidase mutations. *Mol. Genet. Metab.* **104,** 185–188
8. Murphy, K. E., Gysbers, A. M., Abbott, S. K., Tayebi, N., Kim, W. S., Sidransky, E., Cooper, A., Garner, B., and Halliday, G. M. (2014) Reduced glucocerebrosidase is associated with increased α-synuclein in sporadic Parkinson's disease. *Brain* **137,** 834–848
9. Sidransky, E., and Lopez, G. (2012) The link between the GBA gene and parkinsonism. *Lancet Neurol.* **11,** 986–998
10. Sidransky, E., Nalls, M. A., Aasly, J. O., Aharon-Peretz, J., Annesi, G., Barbosa, E. R., Bar-Shira, A., Berg, D., Bras, J., Brice, A., Chen, C. M., Clark, L. N., Condroyer, C., De Marco, E. V., Dürr, A., Eblan, M. J., Fahn, S., Farrer, M. J., Fung, H. C., Gan-Or, Z., Gasser, T., Gershoni-Baruch, R., Giladi, N., Griffith, A., Gurevich, T., Januario, C., Kropp, P., Lang, A. E., Lee-Chen, G. J., Lesage, S., Marder, K., Mata, I. F., Mirelman, A., Mitsui, J., Mizuta, I., Nicoletti, G., Oliveira, C., Ottman, R., Orr-Urtreger, A., Pereira, L. V., Quattrone, A., Rogaeva, E., Rolfs, A., Rosenbaum, H., Rozenberg, R., Samii, A., Samaddar, T., Schulte, C., Sharma, M., Singleton, A., Spitz, M., Tan, E. K., Tayebi, N., Toda, T., Troiano, A. R., Tsuji, S., Wittstock, M., Wolfsberg, T. G., Wu, Y. R., Zabetian, C. P., Zhao, Y., and Ziegler, S. G. (2009) Multicenter analysis of glucocerebrosidase mutations in Parkinson's disease. *New Engl. J. Med.* **361,** 1651–1661
11. Nalls, M. A., Duran, R., Lopez, G., Kurzawa-Akanbi, M., McKeith, I. G., Chinnery, P. F., Morris, C. M., Theuns, J., Crosiers, D., Cras, P., Engelborghs, S., De Deyn, P. P., Van Broeckhoven, C., Mann, D. M. A., Snowden, J., Pickering-Brown, S., Halliwell, N., Davidson, Y., Gibbons, L., Harris, J., Sheerin, U. M., Bras, J., Hardy, J., Clark, L., Marder, K., Honig, L. S., Berg, D., Maetzler, W., Brockmann, K., Gasser, T., Novellino, F., Quattrone, A., Annesi, G., De Marco, E. V., Rogaeva, E., Masellis, M., Black, S. E., Bilbao, J. M., Foroud, T., Ghetti, B., Nichols, W. C., Pankratz, N., Halliday, G., Lesage, S., Klebe, S., Durr, A., Duyckaerts, C., Brice, A., Giasson, B. I., Trojanowski, J. Q., Hurtig, H. I., Tayebi, N., Landazabal, C., Knight, M. A., Keller, M., Singleton, A. B., Wolfsberg, T. G., and Sidransky, E. (2013) A multicenter study of glucocerebrosidase mutations in dementia with Lewy bodies. *JAMA Neurol.* **70,** 727–735
12. McGlinchey, R. P., and Lee, J. C. (2013) Emerging insights into the mechanistic link between α-synuclein and glucocerebrosidase in Parkinson's disease. *Biochem. Soc. Trans.* **41,** 1509–1512
13. Ho, M. W., and O'Brien, J. S. (1971) Gaucher's disease: deficiency of "acid" β-glucosidase and reconstitution of enzyme activity *in vitro*. *Proc. Natl. Acad. Sci. U.S.A.* **68,** 2810–2813
14. Kolter, T., and Sandhoff, K. (2005) Principles of lysosomal membrane digestion: stimulation of sphingolipid degradation by sphingolipid activator proteins and anionic lysosomal lipids. *Annu. Rev. Cell Dev. Biol.* **21,** 81–103
15. Morimoto, S., Kishimoto, Y., Tomich, J., Weiler, S., Ohashi, T., Barranger,

J. A., Kretz, K. A., and O'Brien, J. S. (1990) Interaction of saposins, acidic lipids, and glucosylceramidase. *J. Biol. Chem.* **265,** 1933–1937
16. Vaccaro, A. M., Tatti, M., Ciaffoni, F., Salvioli, R., Maras, B., and Barca, A. (1993) Function of saposin C in the reconstitution of glucosylceramidase by phosphatidylserine liposomes. *FEBS Lett.* **336,** 159–162
17. Wilkening, G., Linke, T., and Sandhoff, K. (1998) Lysosomal degradation on vesicular membrane surfaces: enhanced glucosylceramide degradation by lysosomal anionic lipids and activators. *J. Biol. Chem.* **273,** 30271–30278
18. Yap, T. L., Gruschus, J. M., Velayati, A., Westbroek, W., Goldin, E., Moaven, N., Sidransky, E., and Lee, J. C. (2011) α-Synuclein interacts with glucocerebrosidase providing a molecular link between Parkinson and Gaucher diseases. *J. Biol. Chem.* **286,** 28080–28088
19. Yap, T. L., Velayati, A., Sidransky, E., and Lee, J. C. (2013) Membrane-bound α-synuclein interacts with glucocerebrosidase and inhibits enzyme activity. *Mol. Genet. Metab.* **108,** 56–64
20. Mak, S. K., McCormack, A. L., Manning-Bog, A. B., Cuervo, A. M., and Di Monte, D. A. (2010) Lysosomal degradation of α-synuclein *in vivo*. *J. Biol. Chem.* **285,** 13621–13629
21. Xilouri, M., Brekk, O. R., and Stefanis, L. (2013) α-Synuclein and protein degradation systems: a reciprocal relationship. *Mol. Neurobiol.* **47,** 537–551
22. Yap, T. L., Gruschus, J. M., Velayati, A., Sidransky, E., and Lee, J. C. (2013) Saposin C protects glucocerebrosidase against α-synuclein inhibition. *Biochemistry* **52,** 7161–7163
23. Sardi, S. P., Clarke, J., Kinnecom, C., Tamsett, T. J., Li, L., Stanek, L. M., Passini, M. A., Grabowski, G. A., Schlossmacher, M. G., Sidman, R. L., Cheng, S. H., and Shihabuddin, L. S. (2011) CNS expression of glucocerebrosidase corrects α-synuclein pathology and memory in a mouse model of Gaucher-related synucleinopathy. *Proc. Natl. Acad. Sci. U.S.A.* **108,** 12101–12106
24. Sardi, S. P., Clarke, J., Viel, C., Chan, M., Tamsett, T. J., Treleaven, C. M., Bu, J., Sweet, L., Passini, M. A., Dodge, J. C., Yu, W. H., Sidman, R. L., Cheng, S. H., and Shihabuddin, L. S. (2013) Augmenting CNS glucocerebrosidase activity as a therapeutic strategy for parkinsonism and other Gaucher-related synucleinopathies. *Proc. Natl. Acad. Sci. U.S.A.* **110,** 3537–3542
25. Lieberman, R. L. A. (2011) Guided tour of the structural biology of Gaucher disease: acid-β-glucosidase and saposin c. *Enzyme Res.* **2011,** 973231
26. Heinrich, F., Ng, T., Vanderah, D. J., Shekhar, P., Mihailescu, M., Nanda, H., and Lösche, M. (2009) A new lipid anchor for sparsely tethered bilayer lipid membranes. *Langmuir* **25,** 4219–4229
27. Budvytyte, R., Valincius, G., Niaura, G., Voiciuk, V., Mickevicius, M., Chapman, H., Goh, H. Z., Shekhar, P., Heinrich, F., Shenoy, S., Lösche, M., and Vanderah, D. J. (2013) Structure and properties of tethered bilayer lipid membranes with unsaturated anchor molecules. *Langmuir* **29,** 8645–8656
28. Heinrich, F., and Lösche, M. (2014) Zooming in on disordered systems: neutron reflection studies of proteins associated with fluid membranes. *Biochim. Biophys. Acta* **1838,** 2341–2349
29. Clifton, L. A., Neylon, C., and Lakey, J. H. (2013) Examining protein-lipid complexes using neutron scattering. *Methods Mol. Biol.* **974,** 119–150
30. Shenoy, S., Shekhar, P., Heinrich, F., Daou, M. C., Gericke, A., Ross, A. H., and Lösche, M. (2012) Membrane association of the PTEN tumor suppressor: molecular details of the protein-membrane complex from SPR binding studies and neutron reflection. *PLoS One* **7,** e32591
31. Heinrich, F., Nanda, H., Goh, H. Z., Bachert, C., Lösche, M., and Linstedt, A. D. (2014) Myristoylation restricts orientation of the GRASP domain on membranes and promotes membrane tethering. *J. Biol. Chem.* **289,** 9683–9691
32. McGillivray, D. J., Valincius, G., Heinrich, F., Robertson, J. W. F., Vanderah, D. J., Febo-Ayala, W., Ignatjev, I., Lösche, M., and Kasianowicz, J. J. (2009) Structure of functional *Staphylococcus aureus* α-hemolysin channels in tethered bilayer lipid membranes. *Biophys. J.* **96,** 1547–1553
33. Nanda, H., Datta, S. A. K., Heinrich, F., Lösche, M., Rein, A., Krueger, S., and Curtis, J. E. (2010) Electrostatic interactions and binding orientation of HIV-1 matrix studied by neutron reflectivity. *Biophys. J.* **99,** 2516–2524
34. Pfefferkorn, C. M., Heinrich, F., Sodt, A. J., Maltsev, A. S., Pastor, R. W., and Lee, J. C. (2012) Depth of α-synuclein in a bilayer determined by fluorescence, neutron reflectometry, and computation. *Biophys. J.* **102,** 613–621
35. Clifton, L. A., Johnson, C. L., Solovyova, A. S., Callow, P., Weiss, K. L., Ridley, H., Le Brun, A. P., Kinane, C. J., Webster, J. R. P., Holt, S. A., and Lakey, J. H. (2012) Low resolution structure and dynamics of a colicin-receptor complex determined by neutron scattering. *J. Biol. Chem.* **287,** 337–346
36. Hatty, C. R., Le Brun, A. P., Lake, V., Clifton, L. A., Liu, G. J., James, M., and Banati, R. B. (2014) Investigating the interactions of the 18 kDa translocator protein and its ligand PK11195 in planar lipid bilayers. *Biochim. Biophys. Acta* **1838,** 1019–1030
37. McGillivray, D. J., Valincius, G., Vanderah, D. J., Febo-Ayala, W., Woodward, J. T., Heinrich, F., Kasianowicz, J. J., and Lösche, M. (2007) Molecular-scale structural and functional characterization of sparsely tethered bilayer lipid membranes. *Biointerphases* **2,** 21–33
38. Jiang, Z., de Messieres, M., and Lee, J. C. (2013) Membrane remodeling by α-synuclein and effects on amyloid formation. *J. Am. Chem. Soc.* **135,** 15970–15973
39. Fiaux, J., Bertelsen, E. B., Horwich, A. L., and Wüthrich, K. (2004) Uniform and residue-specific N-15-labeling of proteins on a highly deuterated background. *J. Biomol. NMR* **29,** 289–297
40. Pfefferkorn, C. M., and Lee, J. C. (2010) Tryptophan probes at the α-synuclein and membrane interface. *J. Phys. Chem. B* **114,** 4615–4622
41. Dura, J. A., Pierce, D. J., Majkrzak, C. F., Maliszewskyj, N. C., McGillivray, D. J., Lösche, M., O'Donovan, K. V., Mihailescu, M., Perez-Salas, U., Worcester, D. L., and White, S. H. (2006) AND/R: Advanced neutron diffractometer/reflectometer for investigation of thin films and multilayers for the life sciences. *Rev. Sci. Instrum.* 10.1063/1.2219744
42. Kirby, B. J., Kienzle, P. A., Maranville, B. B., Berk, N. F., Krycka, J., Heinrich, F., and Majkrzak, C. F. (2012) Phase-sensitive specular neutron reflectometry for imaging the nanometer scale composition depth profile of thin-film materials. *Curr. Opin. Colloid Interface Sci.* 10.1016/j.cocis.2011.11.001
43. Ladokhin, A. S. (1999) Analysis of protein and peptide penetration into membranes by depth-dependent fluorescence quenching: theoretical considerations. *Biophys. J.* **76,** 946–955
44. Ankner, J. F., and Majkrzak, C. F. (1992) Subsurface profile refinement for neutron specular reflectivity. *Proc. SPIE* 10.1117/12.130637
45. Shekhar, P., Nanda, H., Lösche, M., and Heinrich, F. (2011) Continuous distribution model for the investigation of complex molecular architectures near interfaces with scattering techniques. *J. Appl. Phys.* **110,** 102216–102216-12
46. Dvir, H., Harel, M., McCarthy, A. A., Toker, L., Silman, I., Futerman, A. H., and Sussman, J. L. (2003) X-ray structure of human acid-β-glucosidase, the defective enzyme in Gaucher disease. *EMBO Rep.* **4,** 704–709
47. Chen, V. B., Arendall, W. B., 3rd, Headd, J. J., Keedy, D. A., Immormino, R. M., Kapral, G. J., Murray, L. W., Richardson, J. S., and Richardson, D. C. (2010) Molprobity: all-atom structure validation for macromolecular crystallography. *Acta Crystallogr. D Biol. Crystallogr.* **66,** 12–21
48. Shaaltiel, Y., Bartfeld, D., Hashmueli, S., Baum, G., Brill-Almon, E., Galili, G., Dym, O., Boldin-Adamsky, S. A., Silman, I., Sussman, J. L., Futerman, A. H., and Aviezer, D. (2007) Production of glucocerebrosidase with terminal mannose glycans for enzyme replacement therapy of Gaucher's disease using a plant cell system. *Plant Biotechnol. J.* **5,** 579–590
49. Guvench, O., Mallajosyula, S. S., Raman, E. P., Hatcher, E., Vanommeslaeghe, K., Foster, T. J., Jamison, F. W., 2nd, and Mackerell, A. D., Jr. (2011) CHARMM additive all-atom force field for carbohydrate derivatives and its utility in polysaccharide and carbohydrate-protein modeling. *J. Chem. Theory Comput.* **7,** 3162–3180
50. Tanner, D. E., Chan, K. Y., Phillips, J. C., and Schulten, K. (2011) Parallel generalized Born implicit solvent calculations with NAMD. *J. Chem. Theory Comput.* **7,** 3635–3642
51. Ulmer, T. S., Bax, A., Cole, N. B., and Nussbaum, R. L. (2005) Structure and dynamics of micelle-bound human α-synuclein. *J. Biol. Chem.* **280,** 9595–9603
52. McIntosh, T. J., and Holloway, P. W. (1987) Determination of the depth of bromine atoms in bilayers formed from bromolipid probes. *Biochemistry* **26,** 1783–1788

53. Qi, X., and Grabowski, G. A. (1998) Acid β-glucosidase: intrinsic fluorescence and conformational changes induced by phospholipids and saposin c. *Biochemistry* **37,** 11544–11554
54. Brumshtein, B., Wormald, M. R., Silman, I., Futerman, A. H., and Sussman, J. L. (2006) Structural comparison of differently glycosylated forms of acid-β-glucosidase, the defective enzyme in Gaucher disease. *Acta Crystallogr. D Biol. Crystallogr.* **62,** 1458–1465
55. Atrian, S., López-Viñas, E., Gómez-Puertas, P., Chabás, A., Vilageliu, L., and Grinberg, D. (2008) An evolutionary and structure-based docking model for glucocerebrosidase-saposin C and glucocerebrosidase-substrate interactions: relevance for Gaucher disease. *Proteins* **70,** 882–891
56. Alattia, J. R., Shaw, J. E., Yip, C. M., and Privé, G. G. (2007) Molecular imaging of membrane interfaces reveals mode of β-glucosidase activation by saposin C. *Proc. Natl. Acad. Sci. U.S.A.* **104,** 17394–17399
57. Bodner, C. R., Dobson, C. M., and Bax, A. (2009) Multiple tight phospholipid-binding modes of α-synuclein revealed by solution NMR spectroscopy. *J. Mol. Biol.* **390,** 775–790
58. Fusco, G., De Simone, A., Gopinath, T., Vostrikov, V., Vendruscolo, M., Dobson, C. M., and Veglia, G. (2014) Direct observation of the three regions in α-synuclein that determine its membrane-bound behaviour. *Nat. Commun.* **5,** 3827
59. Bartels, T., Ahlstrom, L. S., Leftin, A., Kamp, F., Haass, C., Brown, M. F., and Beyer, K. (2010) The N-terminus of the intrinsically disordered protein α-synuclein triggers membrane binding and helix folding. *Biophys. J.* **99,** 2116–2124